Wavepacket Dynamics on One-Dimensional Harmonic Potentials. An Intuitive Approach to the Understanding of Absorption and Luminescence Spectra

Steve Masson, Myriam Triest, and Christian Reber*

Département de chimie, Université de Montréal, C.P. 6128, Succ. Centre-ville, Montréal QC H3C 3J7, Canada, reber@chimie.umontreal.ca

Received September 11, 2000. Accepted January 17, 2001

Abstract: Absorption and luminescence spectra can be used to derive quantitative information about differences in molecular structure between the ground and excited electronic states. Examples illustrate the effect of the harmonic vibrational frequency and the offset of the potential energy minima along one normal coordinate on the observed spectrum. The time-dependent approach to spectroscopy is used, leading to intuitively appealing visual representations.

Introduction

UV–vis absorption and luminescence spectroscopy are techniques encountered throughout undergraduate research. Distinct colors, as observed for example for many transition-metal compounds, provide a directly observable manifestation of transitions between electronic states [1]. Discussions of the theoretical background used to rationalize the observed colors and spectra usually focus on the purely electronic aspects of the transition, that is, on population changes in the molecular orbitals [1, 2]. This view often leads to a qualitatively correct energy order for the expected transitions, and their intensities can be estimated using group theory [2]. It does not, however, explain the fact that the experimentally observed bands are often very broad with widths on the order of thousands of wavenumbers, in contrast to infrared or Raman spectra, which show transitions narrower by approximately three orders of magnitude [2].

The large bands determining the color of many compounds arise from vibronic processes. Sometimes the broad bands in a UV-vis spectrum are resolved into their individual vibronic transitions, allowing the vibrational modes involved in the transition to be identified [3]. The standard treatment of vibronic band shapes, rigorously described for both harmonic and anharmonic (Morse) potential wells in a recent publication at the advanced undergraduate level [4] is based on the separation of electronic and nuclear wave functions and the calculation of overlap integrals to obtain the intensity of each line, as illustrated in Figure 1 where the relevant overlaps are shaded in gray. This separation can appear artificial to students, and the band shapes of absorption and luminescence spectra are not easily recognized to carry important information on structural differences between the initial and final states of an electronic transition.

We present quantitative animations of electronic transitions that lead to calculated band shapes using a time-dependent alternative (but mathematically equivalent [5]) approach to the traditional time-independent Franck–Condon treatment illustrated in Figure 1. The time-dependent animations presented in the following are intuitively appealing and show that key general characteristics of electronic spectra can be deduced without calculating all final-state eigenfunctions and determining their overlap with the eigenfunction of the initial state. The theoretical background has been presented in a recent article in this journal [6] and elsewhere [7, 8]. The vibronic nature of electronic transitions is emphasized by this approach. We have used the animations to discuss band shapes of electronic absorption and luminescence spectra in a class for advanced undergraduate and first-year graduate students and their feedback has encouraged us to make them available in the following. Animations for situations involving multiple electronic states and multidimensional potential-energy surfaces are published elsewhere [9, 10].

Potential Energy Surfaces and Transitions

We discuss the vibronic band shapes of spectra arising from the potential-energy surfaces in Figure 1. The energy is given in wavenumbers (cm^{-1}) as a function of a dimensionless normal coordinate, Q, which does not oblige us to limit our treatment to a specific reduced mass. The conversion of Q from the dimensionless units used here to Ångstrom units is given in ref 11. The potential energy of the ground state is given by:

$$E_{gs} = \frac{1}{2}\hbar\omega_{gs}Q^2 \qquad (1)$$

The potential energy of the excited state is given by:

$$E_{es} = \frac{1}{2}\hbar\omega_{es}\left(Q-\Delta\right)^2 + E_{00} \qquad (2)$$

where $\hbar\omega_{gs}$ and $\hbar\omega_{es}$ denote the vibrational frequencies of the ground and excited states in cm^{-1}. The offset of the potential-energy minima along Q is given as Δ, and E_{00} denotes the energy of the electronic origin, corresponding

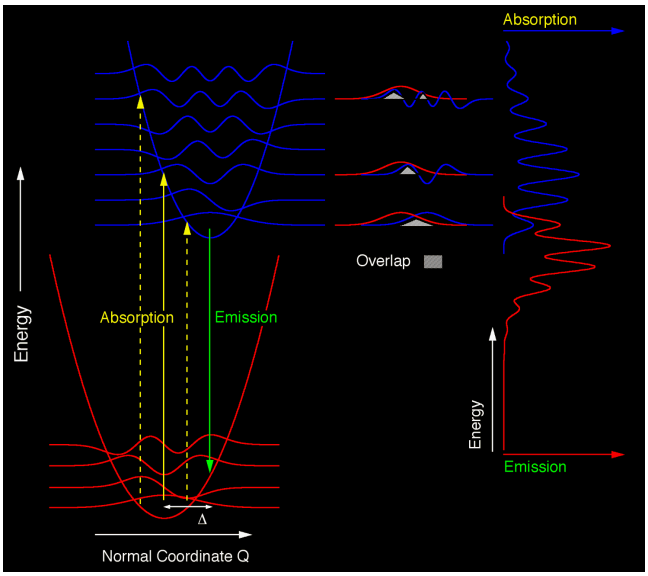

Figure 1. Schematic view of the ground-state potential-energy surface (red) and the excited-state potential energy surface (blue). Absorption and luminescence transitions are given as yellow arrows. The difference between potential-energy minima along the normal coordinate Q is defined as Δ.

to the transition between the lowest energy levels within the two potential wells. We set E_{00} to 20,000 cm^{-1} for the calculations presented in the following. Often the relevant vibrational frequencies and the energy of the electronic origin are known from experimental spectra, but the offset, Δ, can not be directly read from a spectrum and is, therefore, usually not determined, even though it is an important quantity defining the band shape of an experimental spectrum. The offset, Δ, is especially large for transitions involving the transfer of an electron from a bonding to an antibonding orbital (or vice versa), which always leads to a broad band due to the large bond length changes between the ground and excited states. In contrast, narrow bands are observed for many intraconfigurational transitions, for instance, in lanthanide compounds. In general, offsets along several coordinates define the structural differences between the ground and excited states. Such situations can be treated using multiple one-dimensional surfaces [5, 11, 12]. The photochemical reactivity of a molecule is determined by its excited-state structure [12]. Our one-dimensional models illustrate only the simplest possible situations, but they are sufficient to analyze many experimental spectra because the largest bond-length change often occurs along a single normal coordinate, illustrated, for example, by the solution absorption spectrum of the permanganate ion. The animations presented here, therefore, provide the key insight on the factors determining the vibronic band shapes in absorption and luminescence spectra.

Wavepacket Dynamics

In this section we provide quantitative animations of the vibronic dynamics for transitions between the harmonic potential surfaces shown in Figure 1. We systematically vary the offset, Δ, between the two states and their vibrational frequencies $\hbar\omega_{gs}$ and $\hbar\omega_{es}$.

Before an electronic transition, a molecule can be described by its lowest-energy eigenfunction in the initial state of the transition, corresponding to either the red (absorption) or blue (emission) potential well in Figure 1. In the course of an allowed electronic transition, this eigenfunction is transferred from the initial to the final state surface where it is generally away from the minimum of the potential well. This wavepacket evolves with time in the manner shown in Figures 2 to 4 and 6 to 8 for luminescence bands. The most important quantity resulting from the dynamics in Figures 2 to 4 and 6 to 8 is the time-dependent overlap of the moving wave function with the initial wave function at $t = 0$. This time-dependent measure of how different the wave function at time $t > 0$ is from what it was at time $t = 0$ is known as the autocorrelation function [5, 11–13], and its absolute value is shown as a yellow line in the bottom panel of all animations. Its initial value at time $t = 0$ always equals 1. As the time-dependent wave function moves away from its starting position, the autocorrelation first decreases and then increases to a maximum after one vibrational period. We multiply the autocorrelation curve in all the following figures by a damping factor $\exp(-\Gamma^2 t^2)$ to force it to become zero at long times. The parameter Γ defines the width of each individual vibronic transition in a resolved spectrum, but its choice is not critical for the following discussion, which is aimed at unresolved band envelopes. The lowest physically possible value of Γ corresponds to the homogeneous line width, which is related to the lifetime of the excited state by the uncertainty principle [14, 15]. In spectra of molecules in a solution or in the solid state, the line widths are determined by inhomogeneous broadening due to slightly different energy levels for an ensemble of molecules. This inhomogeneous line width is orders of magnitude larger than the intrinsic homogeneous linewidth [15]. The damping factor, Γ, is, therefore, usually a phenomenological description of line widths arising from inhomogeneous broadening. For solution and solid-state spectra, a value on the order of 10 to 100 cm^{-1} is often adequate.

First, we examine a set of animations with different offsets, Δ, between the potential minima, assuming identical vibrational energies for the potentials in Figure 1.

In all following animations, we include only the final-state potential, corresponding to the ground state for an emission transition. The simplest situation is shown in Figure 2. The minima of the ground- and excited-state potentials are not shifted and the Δ value is zero. The wave function placed on the ground-state surface in the electronic transition does not move with time and the autocorrelation simply decreases with the phenomenological damping factor $\exp(-\Gamma^2 t^2)$. This situation applies to all transitions involving identical harmonic potentials and $\Delta = 0$ for the initial and final states, leading to spectra that do not carry vibronic information.

Figure 3 illustrates the situation for a small offset, Δ. The excited-state potential minimum is at a higher value of the normal coordinate Q, whose frequency was chosen as $\hbar\omega_{gs} = \hbar\omega_{es} = 350$ cm^{-1} for this example. The time evolution shown in the animation clearly reveals that the vibronic dynamics and recurrences are observed in the autocorrelation after each vibrational period of 95 fs, a value obtained as $(c\hbar\omega)^{-1}$, where c denotes the speed of light in cm s^{-1}. These

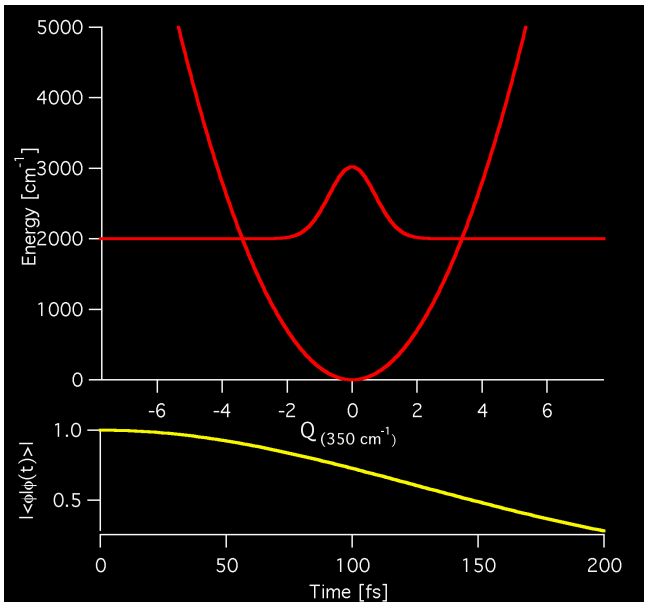

Figure 2. Luminescence transition showing the time evolution of the emitting-state wave function on the ground-state potential surface in the course of the transition. The vibrational frequencies, $\hbar\omega_{gs}$ and $\hbar\omega_{es}$, are identical and set to 350 cm^{-1}. The offset between the potential minima is 0. Download and play animation (Figure2.mov).

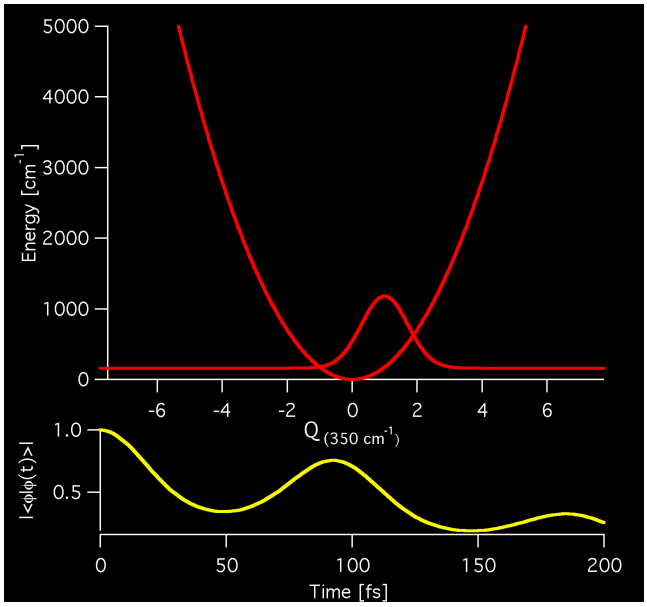

Figure 3. Luminescence transition showing the time evolution of the emitting-state wave function on the ground-state potential surface in the course of the transition. The vibrational frequencies, $\hbar\omega_{gs}$ and $\hbar\omega_{es}$, are identical and set to 350 cm^{-1}. The offset, Δ, between the potential minima is 1. Download and play animation (Figure3.mov).

recurrences are easily seen to occur at times of maximum overlap between the wavepacket at time $t = 0$, given as a thin red line in the top panel, and the moving wavepacket. The Δ value is small and the autocorrelation stays at values significantly higher than zero, even when the wavepacket is the farthest away from its initial position. Figure 4 illustrates a

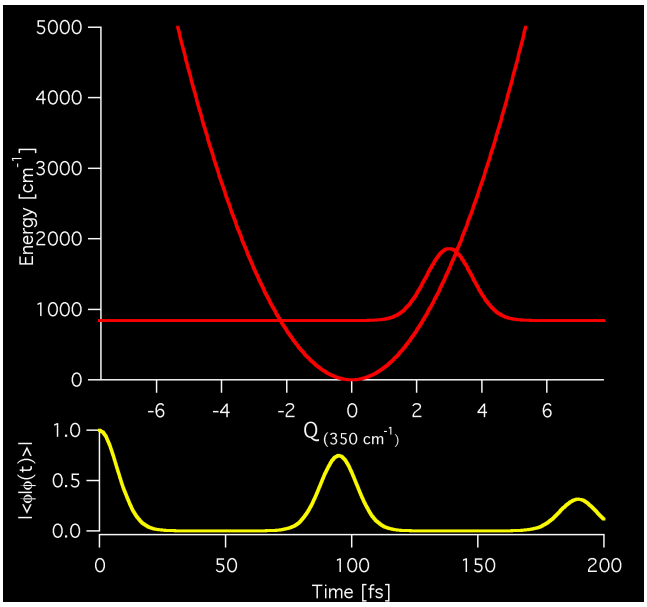

Figure 4. Luminescence transition showing the time evolution of the emitting-state wave function on the ground-state potential surface in the course of the transition. The vibrational frequencies, $\hbar\omega_{gs}$ and $\hbar\omega_{es}$, are identical and set to 350 cm^{-1}. The offset, Δ, between the potential minima is 3. Download and play animation (Figure4.mov).

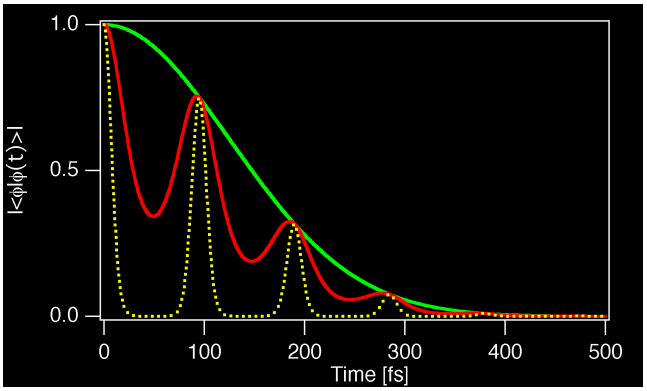

Figure 5. Autocorrelation functions for the models in Figures 2 to 4 for different Δ values: Δ = 3 (yellow dotted trace), Δ = 1 (red trace), and Δ = 0 (green trace).

transition between potentials that are offset by a larger Δ value of 3, but with the same vibrational frequencies as in Figures 2 and 3. The vibrational period stays at the same value of 95 fs, but the motion of the wavepacket is faster than in Figure 3 because the slope of the potential in the starting region of the wavepacket is steeper. This leads to a faster decrease of the autocorrelation with time. The three autocorrelation functions are compared in Figure 5. The initial decrease is faster for large Δ values, but the recurrences occur at the same times, because they are determined by the 350-cm^{-1} vibrational frequency of the ground state. The wavepacket dynamics and autocorrelation functions calculated for harmonic potential-energy surfaces offset by ± Δ are identical. The sign of Δ can, therefore, not be determined from a model based on harmonic potentials, in contrast to anharmonic potentials where a change of the sign of Δ leads to different wavepacket dynamics, a

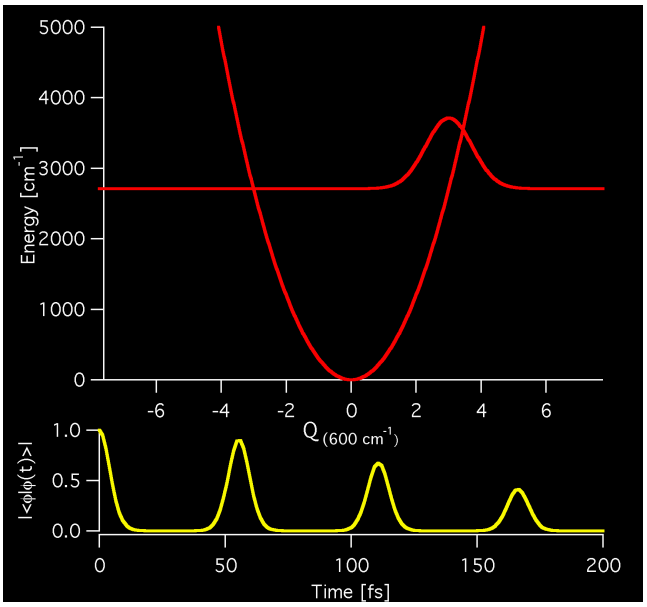

Figure 6. Luminescence transition showing the time evolution of the emitting-state wave function on the ground-state potential surface in the course of the transition. The vibrational frequencies, $\hbar\omega_{gs}$ and $\hbar\omega_{es}$, are identical and set to 600 cm^{-1}. The offset, Δ, between the potential minima is 3. Download and play animation (Figure6.mov).

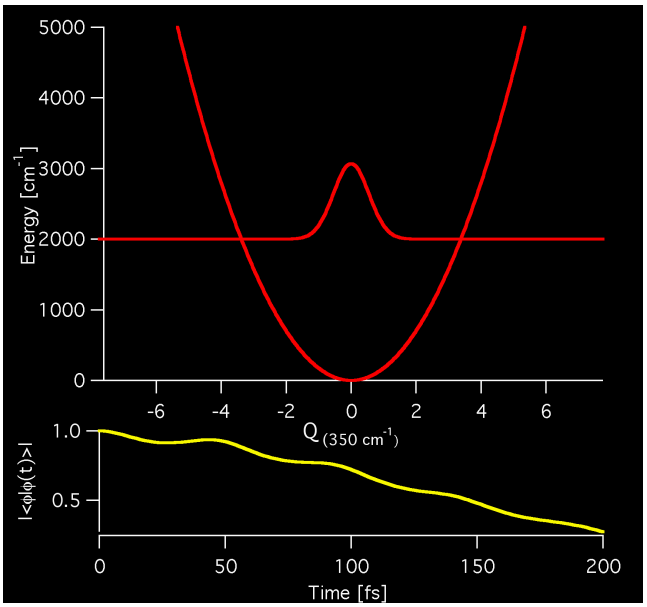

Figure 7. Luminescence transition showing the time evolution of the emitting-state wave function on the ground-state potential surface in the course of the transition. The vibrational frequencies of the excited and ground state are $\hbar\omega_{es} = 600$ cm^{-1} and $\hbar\omega_{gs} = 350$ cm^{-1} respectively. The offset, Δ, between the potential minima is 0. Download and play animation (Figure7.mov).

different autocorrelation, and a different band shape in the spectrum.

Figure 6 illustrates the effect of a higher vibrational frequency on the wavepacket dynamics and autocorrelation functions. The initial motion is faster than for the animations in Figures 3 and 4, a consequence of the steeper slope of the

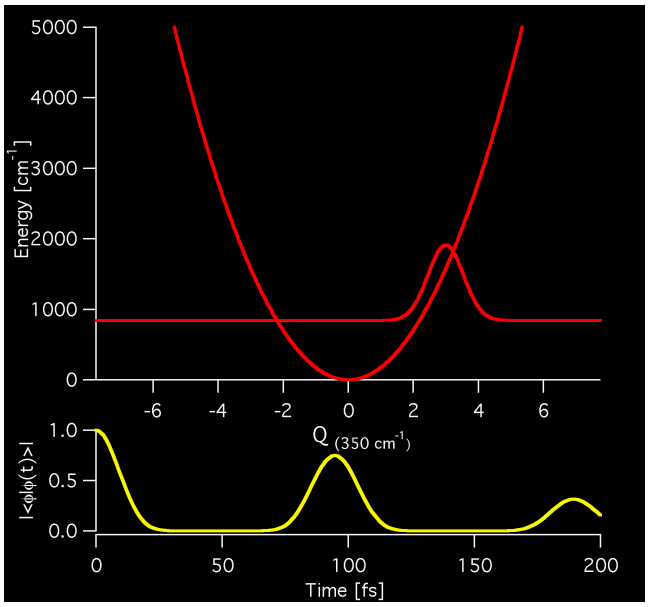

Figure 8. Luminescence transition showing the time evolution of the emitting-state wave function on the ground-state potential surface in the course of the transition. The vibrational frequencies of the excited- and ground-state values of $\hbar\omega_{gs}$ and $\hbar\omega_{es}$ are 350 cm^{-1} and 600 cm^{-1}, respectively. The offset, Δ, between the potential minima is 3. Download and play animation (Figure8.mov).

potential in the regions initially explored by the wavepacket. Recurrences occur after shorter periods than for the preceding animations because of the higher frequency in Figure 6. Maxima occur after 55 fs, the vibrational period corresponding to the frequency of 600 cm^{-1}.

Figures 7 and 8 illustrate situations where the two potentials have different vibrational frequencies. In both situations, the ground-state potential has the same 350-cm^{-1} vibrational frequency as in Figures 2 to 4 and the excited state frequency is 600 cm^{-1}, the value used in Figure 6. Figure 7 shows the wavepacket dynamics for a Δ value of zero. In contrast to Figure 2, Figure 7 shows a distinct time evolution with recurrences occurring after 43 fs. This interval is shorter by roughly a factor of two than the vibrational period for the 350-cm^{-1} vibrational mode. The wavepacket dynamics in Figure 7 is unusual: the two halves of the wave function swap sides, leading to maximum overlap after only half of a vibrational period.

Figure 8 shows a situation that combines different vibrational frequencies for the two potentials with a nonzero Δ value. The wavepacket dynamics is a combination of the effects illustrated in Figure 7 and the simpler vibrational motion in Figures 3, 4, and 6. The autocorrelation is dominated by the recurrences after each vibrational period that correspond to the 350-cm^{-1} mode of the ground state. The shape of these recurrences is slightly different from Figure 4, a consequence of the different frequencies of the initial and final states of the transition, but Figure 9 illustrates that these differences are minor, even for the large change of vibrational frequencies chosen for the model in Figure 7. In general, vibrational frequencies of the ground and excited states vary by much smaller amounts and models based on identical harmonic frequencies for both states provide adequate descriptions of unresolved spectra.

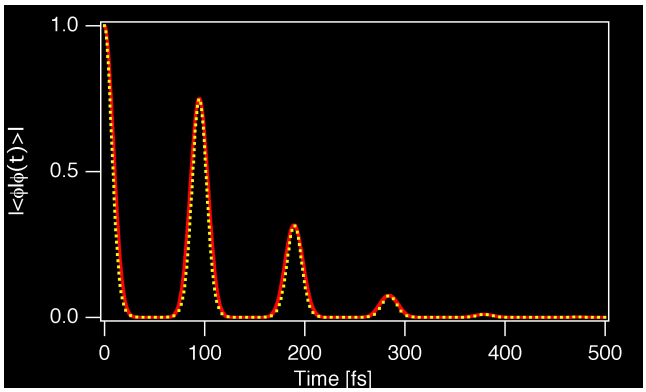

Figure 9. Autocorrelation function of Figures 4 (red trace) and 8 (yellow dotted trace).

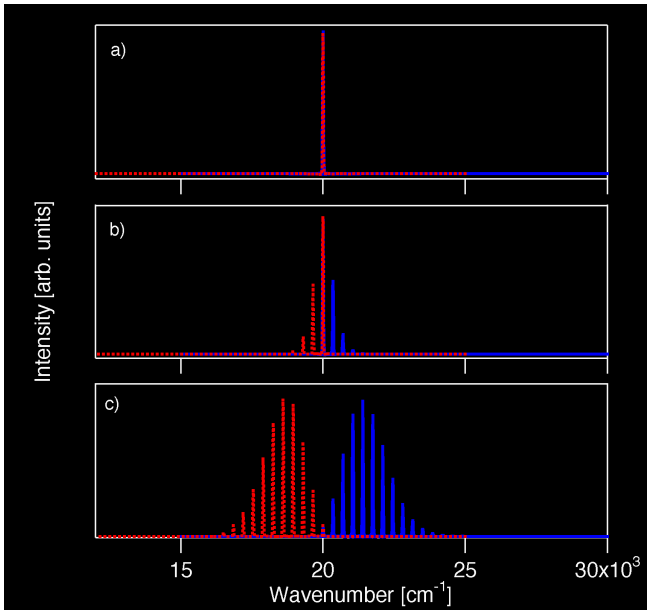

Figure 10. Calculated luminescence (red dotted traces) and absorption (blue traces) of the models in Figures 2 to 4, that is, for different Δ values: (a) Δ = 0, (b) Δ = 1, and (c) Δ = 3.

Calculated Spectra. We present calculated absorption and luminescence spectra corresponding to the transitions schematically illustrated in Figure 1. The absorption and luminescence spectra calculated from the autocorrelation functions in Figures 2 to 4 are shown in Figure 10. The top trace shows that a single line is observed for a Δ value of 0, corresponding to the electronic origin with an identical transition energy for absorption and luminescence. Progressions consisting of peaks separated by 350 cm^{-1} appear for nonzero Δ values. The number of peaks visible in the spectra increases with Δ and the Stokes shift, the energy separation of absorption and excited-state potentials with identical force constants, and luminescence maxima, also increases with Δ. For ground- and excited-state potentials with identical force constants, absorption and luminescence spectra appear as approximate mirror images that overlap at the electronic origin. In experimental spectra obtained from solutions, often only the envelope of the spectra in Figure 10 is observed. This envelope is determined by the decrease of the autocorrelation function at short times, illustrated in Figure 5.

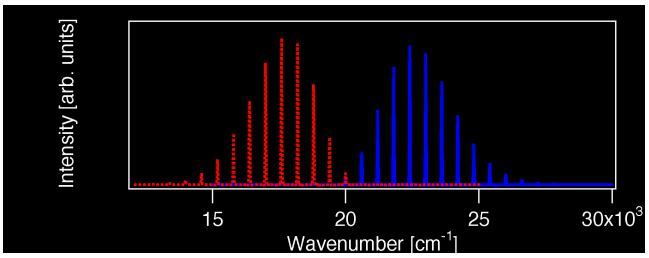

Figure 11. Calculated luminescence (red dotted trace) and absorption (blue trace) of the model in Figure 6 for a Δ value of 3.

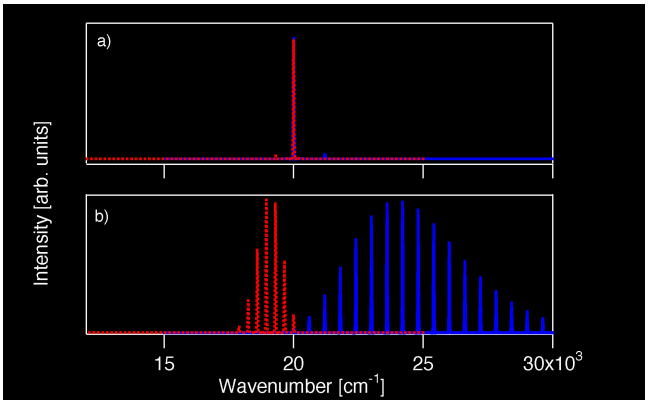

Figure 12. Calculated luminescence (red dotted traces) and absorption (blue traces) of the models in Figure 7 and 8 for different Δ values: (a) Δ = 0 and (b) Δ = 3.

The decrease is fastest for the largest Δ value, leading to the broadest band.

Figure 11 shows calculated absorption and luminescence spectra for potentials with vibrational frequencies of 600 cm^{-1}. A long progression with its members separated by 600 cm^{-1} appears. The overall width of the band is larger than in Figure 10, despite the identical Δ value used in the model calculation, a consequence of the larger separation between the peaks forming the progression.

Figure 12 shows the spectra calculated from the models in Figures 7 and 8. The spectra calculated for Δ equals 0 in Figure 7 are shown in Figure 12a. The main intensity is observed at the electronic origin, similar to Figure 10a. The wavepacket dynamics in Figure 7 leads to an additional peak separated by 700 cm^{-1} from the origin. This energy difference corresponds to two vibrational quanta of the ground-state potential, a consequence of the symmetry of the potential surface and the wave function at time zero. The calculated absorption spectrum in Figure 12a shows an energy difference of 1200 cm^{-1}, corresponding to the double of the excited-state vibrational energy. These additional peaks are weak and unlikely to be observed in unresolved solution spectra, but the wavepacket dynamics easily rationalizes the unusual vibronic structure for this situation.

The effect of different vibrational frequencies and nonzero Δ values is illustrated in Figure 12b. These spectra show that the absorption and luminescence band shapes are no longer mirror images as in Figure 10, as is generally the case if the two states involved in the transition have different potential-energy surfaces.

Acknowledgment. This work was made possible by grants from the Natural Sciences and Engineering Research Council (Canada).

Supporting Material. The animated Figures 2–4 and 6–8 (QuickTime Movie format) may be downloaded individually and are available at (http://dx.doi.org/10.1007/s00897000466a).

References and Notes

1. Butler, I. S.; Harrod, J. F. *Inorganic Chemistry—Principles and Applications;* Benjamin/Cummings: Redwood City, California, 1989.
2. Harris, D. C.; Bertolucci, M. D. *Symmetry and Spectroscopy;* Oxford University Press: Oxford, England, 1978.
3. Brunold, T.; Güdel, H. U. In *Inorganic Electronic Structure and Spectroscopy;* Solomon, E. I.; Lever, A. B. P., Eds.; John Wiley: New York, 1999, Vol. I, pp 253–306.
4. Wright, J. C.; Zielinski, T. J. *J. Chem. Educ.* **1999,** *76,* 1367–1373.
5. Heller, E. J. *Acc. Chem. Res.* **1981,** *14,* 368–375.
6. Nowak, A. M.; Eno, L. *Chem. Educator* [Online] **2000,** *4*, 175–180; DOI 10.1007/s00897000395a.
7. Hansen, J. C.; Kouri, D. J.; Hoffman, D. K. *J. Chem. Educ.* **1997,** *74*, 335–342.
8. Tanner, J. J. *J. Chem. Educ.* **1990,** *67,* 917–921.
9. Triest, M.; Masson, S.; Grey, J. K.; Reber, C. *Phys. Chem. Comm.* [online] **2000,** article 12. avail: http://www.rsc.org/is/journals/current/physchemcomm/pccpub.htm
10. Triest, M.; Bussière, G.; Bélisle, H.; Reber, C. *J. Chem. Educ.* **2000,** *77,* 670–670, full article in the web edition, URL: http://JChemEd.chem.wisc.edu/JCEWWW/Articles/JCENi/JCENi.html (accessed Feb 2001).
11. Zink, J. I.; Kim Shin, K.-S. *Adv. Photochem.* **1991,** *16,* 119–214.
12. Zink, J. I. *Coord. Chem. Rev.* **2001,** *211,* 69–96.
13. Schatz, G. C.; Ratner, M. A. *Quantum Mechanics in Chemistry;* Prentice-Hall: Englewood Cliffs, NJ, 1993.
14. Thomsen, V. B. E. *J. Chem. Educ.* **1995,** *72,* 616–618.
15. Imbusch, G. F.; Kopelman, R. In *Laser Spectroscopy of Solids,* 2nd ed.; Yen, W. M.; Selzer, P. M., Eds.; Topics in Applied Physics 49; Springer: New York, NY, 1986, pp 1–37.